Dalton Transactions

PAPER

View Article Online
View Journal | View Issue

Cite this: *Dalton Trans.*, 2015, **44**, 7679

Comparative investigations of the crystal structure and photoluminescence property of eulytite-type $Ba_3Eu(PO_4)_3$ and $Sr_3Eu(PO_4)_3$†

Haipeng Ji,[a] Zhaohui Huang,*[a] Zhiguo Xia,*[b] Maxim S. Molokeev,[c,d] Xingxing Jiang,[e,f] Zheshuai Lin[e] and Victor V. Atuchin[g,h,i]

Received 17th December 2014,
Accepted 10th March 2015

DOI: 10.1039/c4dt03887h

www.rsc.org/dalton

In this study, the $Ba_3Eu(PO_4)_3$ and $Sr_3Eu(PO_4)_3$ compounds were synthesized and the crystal structures were determined for the first time by Rietveld refinement using powder X-ray diffraction (XRD) patterns. $Ba_3Eu(PO_4)_3$ crystallizes in cubic space group $I\bar{4}3d$, with cell parameters of a = 10.47996(9) Å, V = 1151.01(3) Å^3 and Z = 4; Ba^{2+} and Eu^{3+} occupy the same site with partial occupancies of 3/4 and 1/4, respectively. Besides, in this structure, there exists two distorted kinds of the PO_4 polyhedra orientation. $Sr_3Eu(PO_4)_3$ is isostructural to $Ba_3Eu(PO_4)_3$ and has much smaller cell parameters of a = 10.1203(2) Å, V = 1036.52(5) Å^3. The bandgaps of $Ba_3Eu(PO_4)_3$ and $Sr_3Eu(PO_4)_3$ are determined to be 4.091 eV and 3.987 eV, respectively, based on the UV–Vis diffuse reflectance spectra. The photoluminescence measurements reveal that, upon 396 nm n-UV light excitation, $Ba_3Eu(PO_4)_3$ and $Sr_3Eu(PO_4)_3$ exhibit orange-red emission with two main peaks at 596 nm and prevailing 613 nm, corresponding to the $^5D_0 \rightarrow {}^7F_1$ and $^5D_0 \rightarrow {}^7F_2$ transitions of Eu^{3+}, respectively. The dynamic disordering in the crystal structures contributes to the broadening of the luminescence spectra. The electronic structure of the phosphates was calculated by the first-principles method. The analysis elucidats that the band structures are mainly governed by the orbits of phosphorus, oxygen and europium, and the sharp peaks of the europium f-orbit occur at the top of the valence bands.

1. Introduction

Recently, the rare-earth eulytite-type phosphates $A_3Ln(PO_4)_3$ (A = Ca, Sr, Ba, Pb; Ln = La → Lu, Bi, Y, Sc, In) and related phosphors formed by doping with rare-earth ions have attracted interest due to their specific spectroscopic properties. Initially, the eulytite-type structure was recognized in the mineral $Bi_4(SiO_4)_3$ featuring irregular BiO_6 polyhedra and SiO_4 tetrahedra.[1] Then, with the substitution of P for Si and the charge balancing ($3A^{2+} + Ln^{3+}$) for 4Bi, the formation of the artificial eulytite-type phosphates with a general formula $A_3Ln(PO_4)_3$ is reasonably supposed and the compounds represent an important phase family in the AO–Ln_2O_3–P_2O_5 ternary systems.

Owing to the chemical stablity and mild synthesis conditions, $A_3Ln(PO_4)_3$ are targeted as hosts for various luminescent ions in fabricating phosphors for applications in white light emitting diodes (w-LEDs). Hoogendorp *et al.*[2] have prepared and evaluated the luminescence properties of $(Ba,Sr)_3La(PO_4)_3$:Ce^{3+} phosphors. Xia *et al.*[3] reported the efficient color hue tuning of $(Ba,Sr)_3Lu(PO_4)_3$:Eu^{2+} phosphors by cation substitution. Kuo *et al.*[4] and Wang *et al.*[5] prepared the Ce^{3+}/Tb^{3+} and Ce^{3+}/Mn^{2+} co-doped $Sr_3La(PO_4)_3$ green- and orange-red-emitting phosphors. Zhang *et al.*[6] prepared Eu^{3+}/Tb^{3+} co-doped $Ba_3La(PO_4)_3$ and observed that Tb^{3+} can efficiently transfer the excitation energy to Eu^{3+} and sensitize the Eu^{3+} emission. Hou *et al.*[7] prepared $Ba_3Gd(PO_4)_3$:Tb^{3+} phosphor and studied the energy transfer from Gd^{3+} to the Tb^{3+} dopant ions. You's group found that warm white light emission

[a]*School of Materials Science and Technology, National Laboratory of Mineral Materials, Beijing Key Laboratory of Materials Utilization of Nonmetallic Minerals and Solid Wastes, China University of Geosciences (Beijing), Beijing, 100083, China. E-mail: huang118@cugb.edu.cn; Tel: +86 10 82322186*
[b]*School of Materials Sciences and Engineering, University of Science and Technology Beijing, Beijing 100083, China. E-mail: xiazg@ustb.edu.cn; Tel: +86 10 82377955*
[c]*Laboratory of Crystal Physics, Kirensky Institute of Physics, SB RAS, Krasnoyarsk 660036, Russia*
[d]*Department of Physics, Far Eastern State Transport University, Khabarovsk, 680021 Russia*
[e]*Beijing Center for Crystal R&D, Key Lab of Functional Crystals and Laser Technology of Chinese Academy of Sciences, Technical Institute of Physics and Chemistry, Chinese Academy of Sciences, Beijing 100190, China*
[f]*University of the Chinese Academy of Sciences, Beijing 100049, China*
[g]*Laboratory of Optical Materials and Structures, Institute of Semiconductor Physics, SB RAS, Novosibirsk 630090, Russia*
[h]*Functional Electronics Laboratory, Tomsk State University, Tomsk 634050, Russia*
[i]*Laboratory of Semiconductor and Dielectric Materials, Novosibirsk State University, Novosibirsk 630090, Russia*

† Electronic supplementary information (ESI) available: CIF files giving crystallographic data for $Ba_3Eu(PO_4)_3$ and $Sr_3Eu(PO_4)_3$. See DOI: 10.1039/c4dt03887h

can be directly obtained from various Eu^{2+}/Mn^{2+} co-doped eulytite-type phosphates such as $Sr_3Y(PO_4)_3$,[8] $Sr_3Sc(PO_4)_3$,[9] $Ba_3Lu(PO_4)_3$,[10] and $Ba_3Gd(PO_4)_3$.[11] They further reported that tunable emission can be realized by the efficient energy transfer between the dopant ion Mn^{2+} and the structural ion Tb^{3+} in $Sr_3Tb(PO_4)_3$:Mn^{2+}.[12] Bettinelli *et al.*[13,14] investigated the energy transfer in the $Tb^{3+} \rightarrow Eu^{3+}$ pair in $Sr_3Tb_{0.90}Eu_{0.10}(PO_4)_3$, where the transfer efficiency can be as high as 0.93 and the quantum yield is promising for lighting technology. These interesting results inspire us to prepare hosts with luminescent ion and utilize energy transfer to the dopant to achieve emission color tuning.

The Eu^{3+} is one luminescent ion characterized by orange-red line-type emission from the 4f–4f transition, and Eu^{3+}-doped phosphors commonly act as a red-emitting component in w-LEDs.[15,16] $A_3Eu(PO_4)_3$ (A = Ba, Sr, Ca) belong to eulytite-type phosphates with Eu^{3+} as a structure building ion. These phosphates may act as stable red-emitting phosphors or hosts for other dopants (such as Sm^{3+} or Tb^{3+}). In this study, we synthesized $Ba_3Eu(PO_4)_3$ and $Sr_3Eu(PO_4)_3$, firstly determined their crystal structures by Rietveld refinement, and characterized the physical properties concerning the photoluminescence spectra, diffuse reflectance spectra, bandgap as well as the electronic structure. Close attention was also paid to the exploration of the structural disorder influence on the crystallization and the Eu^{3+} photoluminescence in eulytite phosphates.

2. Experimental and data processing

The high-temperature solid state reaction method conventionally used for eulytite phosphate preparation was employed to crystallize $Ba_3Eu(PO_4)_3$ and $Sr_3Eu(PO_4)_3$. The stoichiometric mixtures of $BaCO_3/SrCO_3$ (Analytical Reagent, A. R.), Eu_2O_3 (99.99%), $NH_4H_2PO_4$ (A. R.) were calcined at 800 °C for 4 h to decompose the carbonate and ammonium phosphates, and then were sintered at 1250 °C for 10 h in the air in a tube furnace. After maintaining at the highest temperature, the furnace was shut down and the samples were slowly cooled together with the furnace. After synthesis, the samples were reground into fine powders.

The X-ray diffraction (XRD) data of the powder samples were collected on an X-ray powder diffractometer (D/max-IIIA, Rigaku, Japan) with a step-wise scanning mode over the 2θ range of 5–120°, using Cu Kα radiation (1.5406 Å) under the operating electric voltage and current of 40 kV and 100 mA, respectively. The acquisition of the XRD patterns, which were submitted to Rietveld refinement, was in the step size of 0.02° and counting time of 3 s per step. The photoluminescence spectra were recorded on a fluorescence spectrophotometer (F-4600, Hitachi, Japan) with a photomultiplier tube operating at 500 V using a 150 W Xe lamp as the excitation source. The diffuse reflection spectra were measured on an UV–Vis–NIR spectrophotometer (UV–3700, Shimadzu, Japan) attached with an integrating sphere. Pure $BaSO_4$ powder was used as a reference for 100% reflectance.

The first-principles electronic structure calculations were performed by CASTEP,[17] a plane-wave pseudopotential total energy package based on the density functional theory (DFT).[18] The functionals developed by Ceperley, Alder, Perdew and Zunger (CA-PZ) in the local density approximation (LDA) form were adopted to describe the exchange–correlation energy.[19] The optimized ultrasoft pseudopotentials[20] were employed to model the effective interaction between the atom cores and valence electrons with Ba $5s^25p^66s^2$, Sr $4s^24p^65s^2$, Eu $5s^25p^64f^76s^2$, P $3s^23p^3$ and O $2s^22p^4$ treated as valence electrons, and this allows the use of a relatively small plane-wave basis set without compromising the computational accuracy. The plane-wave cut-off 500 eV and Monkhorst-Pack[21] *k*-meshes spanning less than 0.04 $Å^{-3}$ in the Brillouin zones were chosen. Moreover, to account for the effect of localized f orbits on the electronic structure, the LDA + U[22] method with the on-site orbital dependent Hubbard U_f = 6 eV for europium was employed in the calculation. In the electronic structure calculation, the disorder of oxygen atoms was handled by virtual crystal approximation (VCA). And, because of the large deviation of electron configuration between Ba(Sr) and Eu, to feature the orbits of Eu in the density of state, two of the Sr(Ba)/Eu sites were defined as Eu and the other six were defined as Sr(Ba) atoms directly in a unit cell. The convergence test shows that the above computational parameters are sufficiently accurate for the purpose of this study.

3. Results and discussion

3.1. Phase formation and structural characteristics

The powder XRD patterns of $Ba_3Eu(PO_4)_3$ and $Sr_3Eu(PO_4)_3$ were collected by the way described above. Previously, their patterns were indexed (PDF no. 29-0162 and 48-0410), but the crystal structures remained unsolved. We therefore performed Rietveld refinements of the two patterns using TOPAS 4.2.[23] Fig. 1 presents the observed (red), calculated (black), and difference (gray) XRD profiles for $Ba_3Eu(PO_4)_3$ and $Sr_3Eu(PO_4)_3$, as refined by Rietveld method. It is found that all peaks in the patterns can be indexed by a cubic cell ($I\bar{4}3d$) with parameters close to those of $Ba_3La(PO_4)_3$,[24] which is also in the eulytite-type structure. The pattern of $Sr_3Eu(PO_4)_3$ sample contains a small amount of impurity peaks, the intensities and positions of which can be fitted by the monoclinic $Sr_9In(PO_4)_7$ (PDF 53-179). The In^{3+} ion has ionic radii similar to that of Eu^{3+}. Thus, it is concluded that the impurity is the $Sr_9Eu(PO_4)_7$ compound. The structure of $Ba_3La(PO_4)_3$ was taken as the starting model for the main phase and was used for Rietveld refinement of $Ba_3Eu(PO_4)_3$ and $Sr_3Eu(PO_4)_3$. The site of Ba(Sr) (16*c* site of the $I\bar{4}3d$ space group) was assumed to be occupied by the Ba(Sr) ion at fixed occupation P = 3/4 and by Eu ion at P = 1/4. With this assumption, the sum of occupancies of all ions in this site is equal to 1.00. Thus, Ba/Eu (Sr/Eu) ions locate in one site and are randomly distributed over the $Ba_3Eu(PO_4)_3$ and $Sr_3Eu(PO_4)_3$ crystals. In the crystals, there is one more disordering process in the oxygen sublattice. In the $Ba_3La(PO_4)_3$

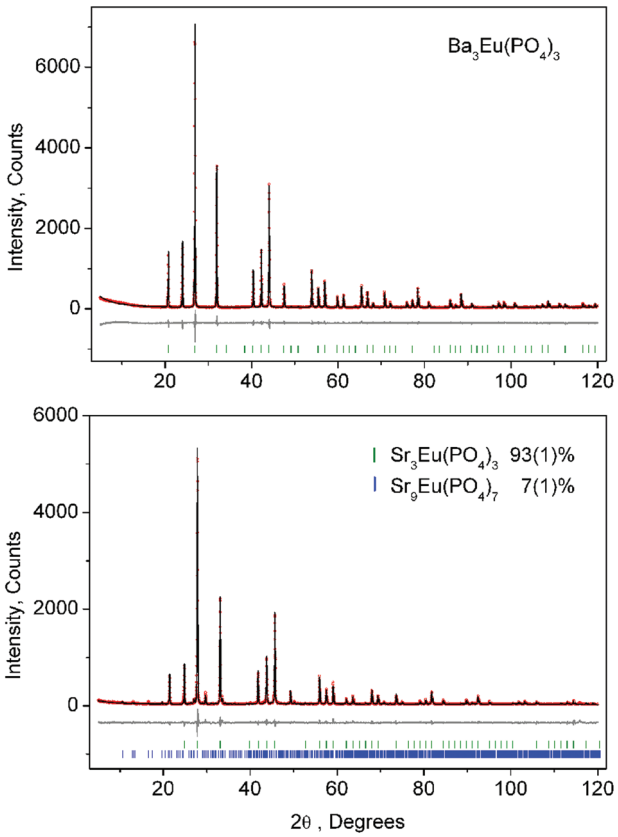

Fig. 1 Observed (red), calculated (black), and difference (gray) XRD profiles of $Ba_3Eu(PO_4)_3$ and $Sr_3Eu(PO_4)_3$ refined by Rietveld method. Bragg reflections are indicated with tick marks.

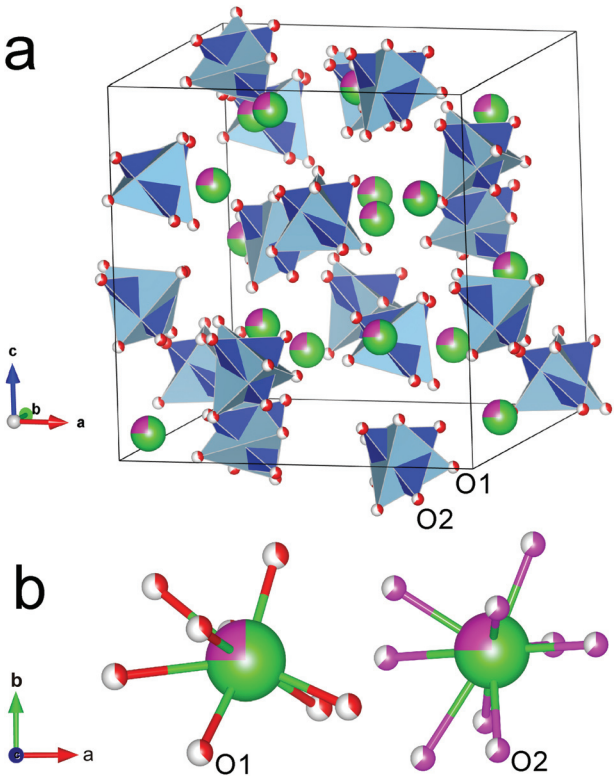

Fig. 2 (a) Schematic crystal structure illustrations of $Ba_3Eu(PO_4)_3$. Ba is green, Eu is pink, $[PO1]_4$ is blue and $[PO2]_4$ is gray-blue. (b) Coordination geometry around the Ba/Eu site viewed along the *c* axis.

crystal, the PO_4 tetrahedron is disordered over two positions with probability 0.65/0.35, that is governed by the bonding requirements of the metal atoms.[24] Our structural model accounts for this and generates two different oxygen sites O1 and O2 corresponding to two different orientations of PO_4 tetrahedrons. The occupancy of O1 ion is equal to x and the occupancy of O2 ion is equal to $(1 - x)$. The value of x took the starting value 0.65 and was then refined. The refinement was stable and ended with relatively low *R*-factors. Fig. 2 depicts the refined crystal structures by VESTA,[25] in which the two different orientations of PO_4 tetrahedrons are diversely colored. The Eu^{3+} ions are isolated by the surrounding PO_4 groups. The final structural parameters together with the details of the refinement are listed in Table 1. The crystallographic information file (CIF) of $Ba_3Eu(PO_4)_3$ and $Sr_3Eu(PO_4)_3$ are given in the ESI.†

Besides, the synthesis of sample with nominal composition of $Ca_3Eu(PO_4)_3$ was also performed using the same procedure as described in the Experimental section. The result, however, was a failure giving the phase mixture of $Ca_3(PO_4)_2$ and $EuPO_4$. In comparison, we noticed that, if Eu^{3+} in the Ln site of $A_3Ln(PO_4)_3$ is completely substituted by La^{3+}, it is possible to crystallize a series of isostructural $Ba_3La(PO_4)_3$,[24,26] $Sr_3La(PO_4)_3$ [27–29] and $Ca_3La(PO_4)_3$.[30] Actually, the preparation of

Table 1 Main parameters of the processing and refinement of $Ba_3Eu(PO_4)_3$ and $Sr_3Eu(PO_4)_3$

Compound	$Ba_3Eu(PO_4)_3$	$Sr_3Eu(PO_4)_3$
Space Group	$I\bar{4}3d$	$I\bar{4}3d$
a/Å	10.47996(9)	10.1203(2)
V/Å^3	1151.01(3)	1036.52(5)
Z	4	4
2θ-interval/°	5–120	5–120
No. of rflns	87	79
No. of params of refinement	36	62
R_{wp} (%)	9.40	13.31
R_p (%)	7.19	9.48
χ^2	0.91	1.12
R_B (%)	1.75	1.66

$Ca_3Eu(PO_4)_3$ has been reported by firing at 1400 °C for 4 days followed by air quenching,[31] which is practically stringent. In the present case of $A_3Eu(PO_4)_3$, when Ba^{2+} is fully substituted by Sr^{2+}, the cell volume considerably decreases from 1151.01(3) to 1036.52(5) Å^3, while the cell volume of $Ca_3Eu(PO_4)_3$ was reported to be 960.63 Å^3.[31] Thus, it is assumed that the ion radius ratio of A^{2+}/Ln^{3+} dominates the phase formation ability of pure $A_3Ln(PO_4)_3$, and the Ca^{2+} with the effective radius of 1.18 Å (CN = 9)[32] fails to fulfil the ratio requirement. Here, we would like to further summarize the reports on the eulytite phosphate $A_3Ln(PO_4)_3$ structures, where A site is Ba, Sr, or Ca,

Table 2 Reported eulytite phosphates $A_3Ln(PO_4)_3$, A = Ba, Sr, or Ca[a]

	A = Ba, Sr, or Ca		
Compounds	Ba	Sr	Ca
$A_3Bi(PO_4)_3$	Y[33,34]	Y[35–37]	Y[24,38,39]
$A_3Y(PO_4)_3$	Y[40–42]	Y[8,43,44]	Y[45,46] (quench)
$A_3La(PO_4)_3$	Y[6,26,47,48]	Y[4,27–29,49,50]	Y[30] (quench)
$A_3Lu(PO_4)_3$	Y[10,51,52]	Y[53]	N
$A_3Sc(PO_4)_3$	Y[54]	Y[9]	Y[55]
$A_3Gd(PO_4)_3$	Y[7,11,56,57]	Y[58–61]	Y[62] (quench)
$A_3Tb(PO_4)_3$	Y[63]	Y[12–14]	N
$A_3Eu(PO_4)_3$	Y	Y	Y[31] (quench)

[a] Y indicates that the compound can be purely crystallized; N indicates that the nominal compound cannot be purely crystallized or has not been reported on.

and Ln site is Bi, Y, La, Lu, Sc, Gd, Tb, or Eu, as shown in Table 2. Predominantly, compounds with A = Ba, Sr, Ca can form pure eulytite phases. The $A_3Ln(PO_4)_3$ (Ln = Lu and Tb) with A = Ba, Sr can form a pure phase; while when A = Ca, the formation of a eulytite structure can be achieved only by developed processing such as quenching. In the eulytite-type structure, the A and Ln ions share the same site and, the crystallization is problematic when smaller Ca^{2+} and relatively big Ln^{3+} ions are combined.

Previously, Barbier *et al.*[24] performed refinements of $Ca_3Bi(PO_4)_3$ and $Ba_3La(PO_4)_3$ using neutron diffraction data, and found that the oxygen sublattice disorder in the type of rotational disorder of the tetrahedral groups can be expected to occur in all mixed metal eulytites. The reason is intrinsically associated with different metal–oxygen bond lengths and most eulytite phases are thermodynamically stable only at high temperatures. The presence of a heavy metal atom and the lone-pair bonding stabilize the eulytite structure at lower temperature and reduce the structural disorder degree by retaining the oxygen atoms in positions close to those observed in $Bi_4(SiO_4)_3$. Large metal atoms such as Ba and Sr appear to have a stabilizing effect on the structure, whereas the Ca analog can be purely obtained only by quenching.[31]

3.2. UV–Vis diffuse reflectance spectra and bandgap determination

Bandgap is a basic material property of a compound. For a powder sample, the diffuse reflectance measurement is a convenient technique to evaluate the optical absorption properties. Fig. 3(a) showed the UV–Vis reflection spectra of $Ba_3Eu(PO_4)_3$ and $Sr_3Eu(PO_4)_3$. The Tauc plot based on the Kubelka–Munk function (eqn (1)) is used to estimate the bandgaps:

$$(h\nu\alpha)^{1/n} = A(h\nu - E_g) \quad (1)$$

Here, h is Planck's constant, ν is frequency of vibration, α is absorption coefficient, E_g is bandgap, and A is a constant. Exponent value n denotes the nature of electron transition: n = 1/2 for direct allowed transition and n = 2 for indirect allowed

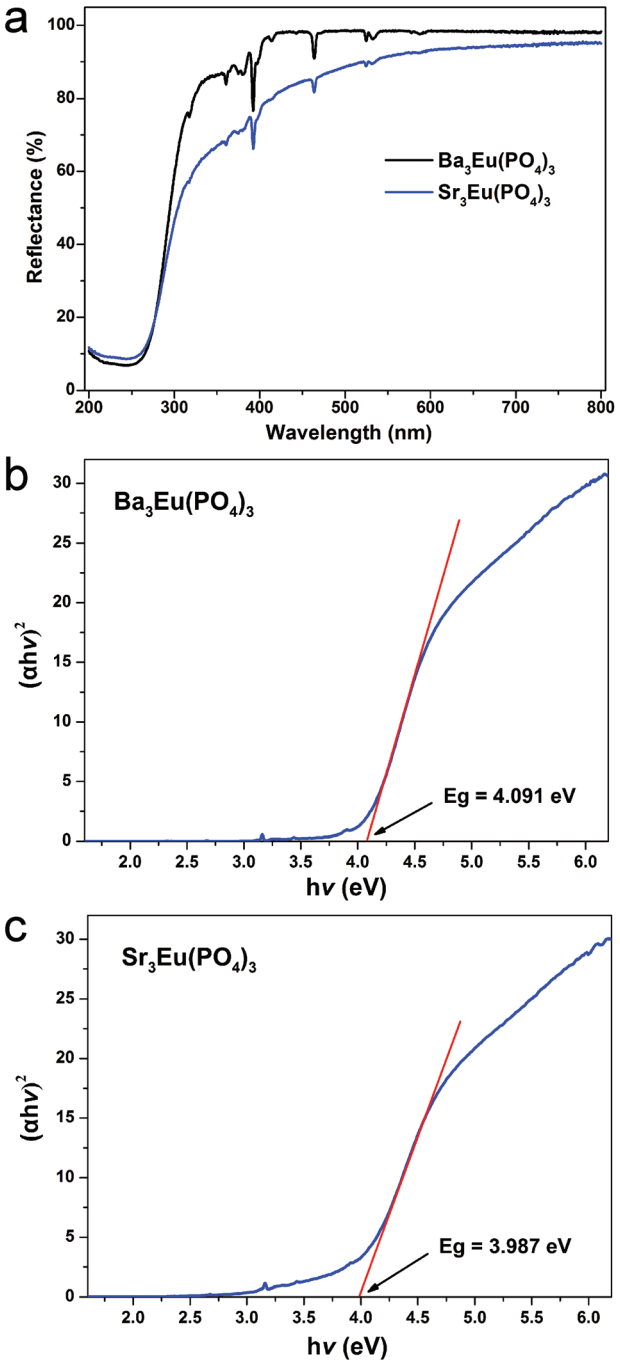

Fig. 3 Diffuse reflectance spectra of $Ba_3Eu(PO_4)_3$ and $Sr_3Eu(PO_4)_3$ (a), and Tauc's plot of $(\alpha h\nu)^2$ as a function of photon energy ($h\nu$) for $Ba_3Eu(PO_4)_3$ (b) and $Sr_3Eu(PO_4)_3$ (c).

transition. Using the eqn (1), the $(h\nu\alpha)^{1/n}$ is plotted against the $h\nu$. A line is drawn tangent to the point of inflection on the curve to determine the bandgap value E_g. Since we do not know the nature of transition in these compounds, both n = 1/2 and 2 were examined. From Fig. 3(a), at 310 nm the reflectance drops steeply with respect to wavelength, and the bandgaps can be roughly estimated to be 1240/310 = 4 eV;

here, the case of n = 1/2 generate results closer to the above value. Thus, as shown in Fig. 3(b, c), the bandgaps of $Ba_3Eu(PO_4)_3$ and $Sr_3Eu(PO_4)_3$ were finally determined to be 4.091 eV and 3.987 eV, respectively.

3.3. Photoluminescence spectra analysis

Both of the powder products are of white color under sunlight and emit orange-red light under the 365 nm UV light illumination which suggests similar spectroscopic properties. Thus, the following luminescence investigation is concentrated on one of them, namely $Ba_3Eu(PO_4)_3$. Fig. 4 depicts the photoluminescence emission and excitation spectra at room temperature. Upon the 396 nm excitation, the emission spectrum of $Ba_3Eu(PO_4)_3$ (Fig. 4a) contains the typical transitions of Eu^{3+} from the excited ^5D_o energy level to the ground state ^7F_j (j = 0, 1, 2, 3, 4) multiplets.[16,64,65] Two main peaks at 613 nm and 596 nm exhibit the relatively high intensity corresponding to the allowed $^5D_0 \rightarrow {}^7F_2$ electric-dipole transition (ED) and $^5D_0 \rightarrow {}^7F_1$ magnetic-dipole transition (MD), respectively. The ED transition is super sensitive to the Eu^{3+} site symmetry, whereas the MD one is insensitive to that, and this behavior can be used to predict the Eu^{3+} position symmetry. In the considered case, the prevailing peak at 613 nm dominates the emission, suggesting that Eu^{3+} in the crystal occupies a noncentrosymmetric site with low symmetry. Indeed, crystal structure refinement indicates that the Eu and Ba ions share the same site (x', x', x') (x' = 0.0634) in $Ba_3Eu(PO_4)_3$, which has a 16c Wykoff position and site symmetry of ".3.". Therefore, only a 3-fold axis goes through this position and there is no inversion center. The observed emission character of Eu^{3+} is in line with structural information from the XRD refinement. Moreover, the emission bands are relatively wide compared with Eu^{3+} emission in other crystalline matrices; herein, the Eu^{3+} ion shares the same crystallographic site with the Ba^{2+} (or Sr^{2+}) ion and is coordinated with oxygen occupied in disordered sublattice sites. The specific dynamic disordering in the eulytite-type compounds is believed to induce much more energy level splitting of Eu^{3+}, which then causes the broadening of the luminescence emission spectrum of Eu^{3+}. The excitation spectrum monitored at 613 nm is shown in Fig. 4b which contains a series of sharp excitation bands between 280 and 420 nm. These sharp bands originate from the intra-configurational 4f–4f transitions in Eu^{3+}, namely, $^7F_0$ to ^5F_j, $^5H_6$, $^5H_3$, $^5D_4$, $^5L_8$, $^5G_3$, $^5G_2$, $^5L_6$, and $^5D_3$ at wavelengths 297, 317, 326, 362, 365, 376, 382, 394, and 413 nm, respectively.[48] The $Ba_3Eu(PO_4)_3$ luminescence is observed to be similar to that of $Ba_3La(PO_4)_3$:Eu^{3+}.[48] The photoluminescence spectra of $Sr_3Eu(PO_4)_3$ (Fig. 4c) is almost similar to that of $Ba_3Eu(PO_4)_3$ because, in both the isostructural phosphates, the luminescence property originates from the Eu^{3+} ion which experiences the same site symmetry.

3.4. Electronic structure analysis

The $Ba_3Eu(PO_4)_3$ and $Sr_3Eu(PO_4)_3$ exhibit similar electronic structures. The partial density of states (PDOS) projected onto the constituent atoms of them are plotted in Fig. 5. Some characteristic features can be accordingly deduced: (1) the PDOS of europium in different spin states split seriously from each other due to the strong spin-related correlation for the f-electrons, while no obvious spin-splitting was observed for other elements; (2) the Ba 5s, Sr 4s,

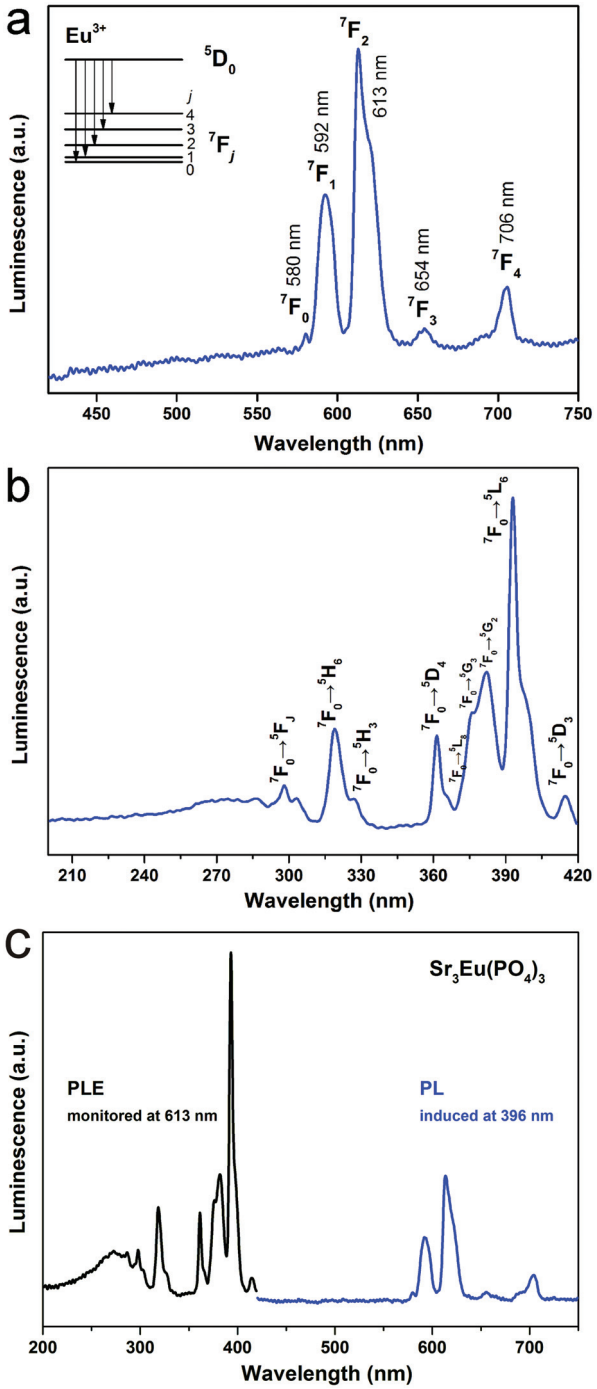

Fig. 4 (a) Photoluminescence emission (PL) spectrum of $Ba_3Eu(PO_4)_3$ under 396 nm light excitation, (b) photoluminescence excitation (PLE) spectrum of $Ba_3Eu(PO_4)_3$ monitored at 613 nm, and (c) photoluminescence emission and excitation spectra of $Sr_3Eu(PO_4)_3$.

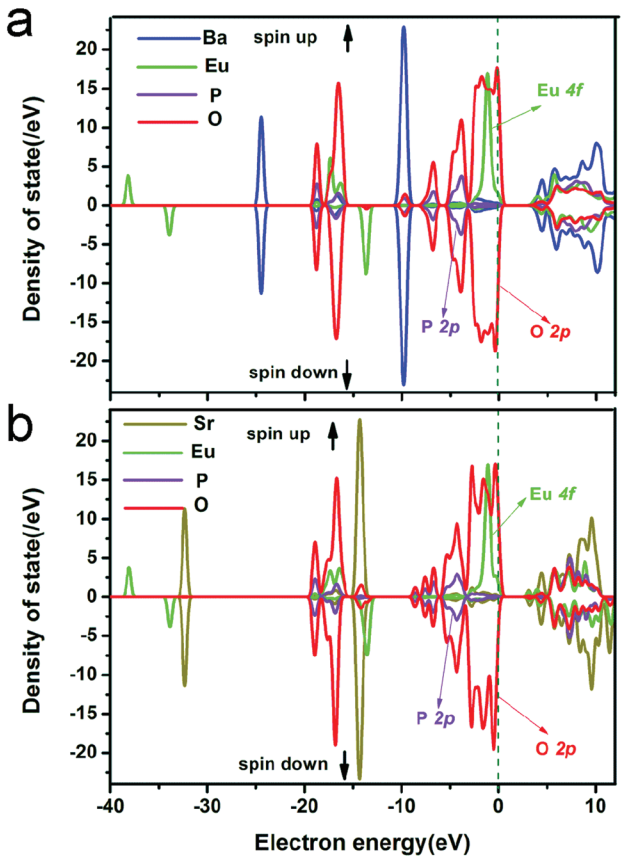

Fig. 5 The projected density of states on the constituent atoms of (a) $Ba_3Eu(PO_4)_3$ and (b) $Sr_3Eu(PO_4)_3$.

and Eu 5s orbits are deeply located in the inner energy level below −20 eV, which is difficult to be excited by the external perturbation of the optical electric field, indicating that they almost make no contribution to the optical properties related to the electronic transition across the forbidden band. These orbits hybridize little with each other, verifying that they almost do not participate in the formation of the covalent bonds; (3) the energy states between −20 eV and −9 eV mainly consist of Ba 5p (Sr 4p), Eu 5p, P 3s and O 2s orbits. The strong hybridization between the Eu, P and O orbits in this region indicates the strongly covalent P–O and Eu–O interactions. However, the sharp peaks of Ba 5p (Sr 4p) orbitals occur at −10 eV (−14 eV), proving the strong ionicity of barium (strontium); and (4) the energy levels near the forbidden bands are mainly composed of P 3p, O 3p and Eu 4f orbits. This indicates that the optical property is dominantly determined by the electron transitions within $(PO_4)^{3-}$ groups and the f–f transition of europium. Especially a sharp peak of the Eu 4f orbital of the spin-up electrons occupies the top of the valence bands and contributes a lot to the bottom of the conduction bands, verifying that the electron transition to the $^5D_0$ configuration dominates the photoluminescence properties of $Ba_3Eu(PO_4)_3$ and $Sr_3Eu(PO_4)_3$.

4 Conclusions

$Ba_3Eu(PO_4)_3$ and $Sr_3Eu(PO_4)_3$ can be successfully synthesized at 1250 °C *via* the high temperature solid state reaction method followed by furnace-cooling while the $Ca_3Eu(PO_4)_3$ analog cannot purely crystallize in the same way. The ion radius ratio of A^{2+}/Ln^{3+} dominates the phase formation ability of pure $A_3Ln(PO_4)_3$. Rietveld refinements show that $Ba_3Eu(PO_4)_3$ and $Sr_3Eu(PO_4)_3$ are isostructural, both holding the cubic eulytite-type disordered structure in space group $I\bar{4}3d$. $Ba_3Eu(PO_4)_3$ has cell parameters of a = 10.47996(9) Å, V = 1151.01(3) Å^3, Z = 4, while $Sr_3Eu(PO_4)_3$ has much smaller cell parameters of a = 10.1203(2) Å, V = 1036.52(5) Å^3. Based on the diffuse reflectance spectra, the bandgaps of $Ba_3Eu(PO_4)_3$ and $Sr_3Eu(PO_4)_3$ are estimated to be about 4.091 eV and 3.987 eV, respectively. Upon 396 nm UV light excitation, $Ba_3Eu(PO_4)_3$ and $Sr_3Eu(PO_4)_3$ exhibit orange-red emission with two main peaks at 596 nm and 613 nm, corresponding to the $^5D_0 \rightarrow {}^7F_1$ and $^5D_0 \rightarrow {}^7F_2$ transitions of Eu^{3+}, respectively. The 613 nm emission dominates the photoluminescence property because the Eu^{3+} ion occupies the 16c Wykoff position in the crystal which has no inversion center. The electronic structure calculation verifies that the Eu 4f orbital mainly occupies the top of the valence bands and the bottom of the conduction bands, and the electron transition to the $^5D_0$ configuration dominates the photoluminescence properties.

Acknowledgements

This work was supported by the National Natural Science Foundations of China (grant no. 51032007, no. 51002146, no. 51272242), the Research Fund for the Doctoral Program of Higher Education of China (grant no. 20130022110006), Natural Science Foundations of Beijing (2132050), and the Program for New Century Excellent Talents in the University of the Ministry of Education of China (NCET-12-0950), Beijing Nova Program (Z131103000413047) and Beijing Youth Excellent Talent Program (YETP0635). VVA is partly supported by the Ministry of Education and Science of the Russian Federation.

References

1 G. Menzer, *Z. Kristallogr.*, 1931, **78**, 136–163.
2 M. F. Hoogendorp, W. J. Schipper and G. Blasse, *J. Alloys Compd.*, 1994, **205**, 249–251.
3 Z. Wang, Z. Xia, M. S. Molokeev, V. V. Atuchin and Q. Liu, *Dalton Trans.*, 2014, **43**, 16800–16804.
4 T. W. Kuo and T. M. Chen, *J. Electrochem. Soc.*, 2010, **157**, J216–J220.
5 Z. Wang, S. Lou and P. Li, *J. Lumin.*, 2014, **156**, 87–90.
6 C. H. Zhang, H. B. Liang, S. Zhang, C. M. Liu, D. J. Hou, L. Zhou, G. B. Zhang and J. Y. Shi, *J. Phys. Chem. C*, 2012, **116**, 15932–15937.

7 D. J. Hou, H. B. Liang, M. B. A. Xie, X. M. Ding, J. P. Zhong, Q. Su, Y. Tao, Y. Huang and Z. H. Gao, *Opt. Express*, 2011, **19**, 11071–11083.
8 N. Guo, Y. Huang, M. Yang, Y. Song, Y. Zheng and H. You, *Phys. Chem. Chem. Phys.*, 2011, **13**, 15077–15082.
9 N. Guo, Y. C. Jia, W. Lu, W. Z. Lv, Q. Zhao, M. M. Jiao, B. Q. Shao and H. P. You, *Dalton Trans.*, 2013, **42**, 5649–5654.
10 N. Guo, Y. J. Huang, Y. C. Jia, W. Z. Lv, Q. Zhao, W. Lu, Z. G. Xia and H. P. You, *Dalton Trans.*, 2013, **42**, 941–947.
11 N. Guo, W. Lu, Y. C. Jia, W. Z. Lv, Q. Zhao and H. P. You, *ChemPhysChem*, 2013, **14**, 192–197.
12 Y. C. Jia, W. Lu, N. Guo, W. Z. Lu, Q. Zhao and H. P. You, *Phys. Chem. Chem. Phys.*, 2013, **15**, 6057–6062.
13 M. Bettinelli, A. Speghini, F. Piccinelli, J. Ueda and S. Tanabe, *Opt. Mater.*, 2010, **33**, 119–122.
14 M. Bettinelli, F. Piccinelli, A. Speghini, J. Ueda and S. Tanabe, *J. Lumin.*, 2012, **132**, 27–29.
15 D. Kang, H. S. Yoo, S. H. Jung, H. Kim and D. Y. Jeon, *J. Phys. Chem. C*, 2011, **115**, 24334–24340.
16 V. V. Atuchin, A. S. Aleksandrovsky, O. D. Chimitova, T. A. Gavrilova, A. S. Krylov, M. S. Molokeev, A. S. Oreshonkov, B. G. Bazarov and J. G. Bazarova, *J. Phys. Chem. C*, 2014, **118**, 15404–15411.
17 S. J. Clark, M. D. Segall, C. J. Pickard, P. J. Hasnip, M. J. Probert, K. Refson and M. C. Payne, *Z. Kristallogr.*, 2005, **220**, 567–570.
18 M. C. Payne, M. P. Teter, D. C. Allan, T. A. Arias and J. D. Joannopoulos, *Rev. Mod. Phys.*, 1992, **64**, 1045–1097.
19 B. J. A. D. M. Ceperley, *Phys. Rev. Lett.*, 1980, **45**, 566.
20 A. M. Rappe, K. M. Rabe, E. Kaxiras and J. D. Joannopoulos, *Phys.Rev. B: Condens. Matter*, 1990, **41**, 1227–1230.
21 J. D. P. H. J. Monkhorst, *Phys. Rev. B: Solid State*, 1976, **13**, 5188–5192.
22 M. Cococcioni and S. de Gironcoli, *Phys. Rev. B: Condens. Matter Mater. Phys.*, 2005, **71**, 16.
23 B. A. T. V4, *General profile and structure analysis software for powder diffraction data. User's Manual*. Bruker AXS, Karlsruhe, Germany, 2008.
24 J. Barbier, *J. Solid State Chem.*, 1992, **101**, 249–256.
25 F. I. K. Momma, *J. Appl. Crystallogr.*, 2011, **44**, 1272–1276.
26 R. J. Yu, H. M. Noh, B. K. Moon, B. C. Choi, J. H. Jeong, H. S. Lee, K. Jang and S. S. Yi, *J. Lumin.*, 2014, **145**, 717–722.
27 J. Barbier, J. E. Greedan, T. Asaro and G. J. McCarthy, *Eur. J. Solid State Inorg. Chem.*, 1990, **27**, 855–867.
28 F. H. Wang, D. Z. Zhou, S. Y. Ma, H. W. Yu, P. L. Li and Z. P. Yang, *J. Alloys Compd.*, 2011, **509**, 4824–4827.
29 P. L. Li, Z. J. Wang, Z. P. Yang and Q. L. Guo, *J. Electrochem. Soc.*, 2012, **159**, H307–H311.
30 W. Jungowska, *Solid State Sci.*, 2002, **4**, 229–232.
31 M. Pfoertsch, Penn State University, University Park, Pennsylvania, USA. ICDD Grant-in-Aid, 1977.
32 R. D. Shannon, *Acta Crystallogr., Sect. A: Found. Crystallogr.*, 1976, **32**, 751–767.
33 F. Yang, H. Ma, Y. Liu, Q. Liu, Z. Yang and Y. Han, *Ceram. Int.*, 2013, **39**, 2127–2130.
34 F. Yang, Z. Yang, Q. Yu, Y. Liu, X. Li and F. Lu, *Spectrochim. Acta, Part A*, 2013, **105**, 626–631.
35 Y. F. Liu, Y. J. Ding and Z. M. Peng, *Opt. Eng.*, 2014, **53**, 3.
36 G. Y. Dong, H. X. Ma, Y. F. Liu, Z. P. Yang and Q. B. Liu, *Opt. Commun.*, 2012, **285**, 4097–4101.
37 Z. P. Yang, Y. Han, Y. C. Song, Y. H. Zhao and P. F. Liu, *J. Rare Earths*, 2012, **30**, 1199–1202.
38 M. M. Jiao, N. Guo, W. Lu, Y. C. Jia, W. Z. Lv, Q. Zhao, B. Q. Shao and H. P. You, *Dalton Trans.*, 2013, **42**, 12395–12402.
39 D. Y. Yu, Y. J. Liang, M. F. Zhang, M. H. Tong, Q. Wang, J. W. Zhao, J. M. Wu, G. G. Li and C. J. Yan, *J. Mater. Sci.: Mater. Electron.*, 2014, **25**, 3526–3531.
40 Q. B. Liu, Y. F. Liu, Y. J. Ding, Z. M. Peng, X. D. Tian, Q. M. Yu and G. Y. Dong, *Ceram. Int.*, 2014, **40**, 10125–10129.
41 Z. P. Yang, P. F. Liu, J. J. Li, Q. Yang, L. Lv and Y. H. Zhao, *J. Alloys Compd.*, 2013, **578**, 118–120.
42 C. H. Huang, T. W. Kuo and T. M. Chen, *Opt. Express*, 2011, **19**, A1–A6.
43 Y. C. Jia, W. Lu, N. Guo, W. Z. Lu, Q. Zhao and H. P. You, *Chem. Commun.*, 2013, **49**, 2664–2666.
44 J. Y. Wang, J. B. Wang and P. Duan, *J. Lumin.*, 2014, **145**, 1–5.
45 K. Fukuda, T. Wata and T. Niwa, *J. Solid State Chem.*, 2006, **179**, 3420–3428.
46 A. Matraszek and E. Radominska, *J. Therm. Anal. Calorim.*, 2014, **117**, 101–108.
47 N. Sharova, H. Fjellvag and T. Norby, *Solid State Ionics*, 2009, **180**, 338–342.
48 R. Yu, H. M. Noh, B. K. Moon, B. C. Choi, J. H. Jeong, K. Jang, S. S. Yi and J. K. Jang, *J. Alloys Compd.*, 2013, **576**, 236–241.
49 X. G. Zhang, C. Y. Zhou, J. H. Song, L. Y. Zhou and M. L. Gong, *J. Alloys Compd.*, 2014, **592**, 283–287.
50 Z. J. Wang, S. Q. Lou and P. L. Li, *J. Alloys Compd.*, 2014, **586**, 536–541.
51 C. Jin, H. X. Ma, Y. F. Liu, Q. B. Liu, G. Y. Dong and Q. M. Yu, *J. Alloys Compd.*, 2014, **613**, 275–279.
52 X. G. Zhang, J. L. Zhang and M. L. Gong, *Opt. Mater.*, 2014, **36**, 850–853.
53 N. Guo, Y. H. Zheng, Y. C. Jia, H. Qiao and H. P. You, *J. Phys. Chem. C*, 2012, **116**, 1329–1334.
54 D. Krabbenhoft and G. McCarthy, North Dakota State University, Fargo, North Dakota, USA. ICDD Grant-in-Aid, 1982.
55 W. E. A. Wetzel, Mineral.-Petrograph. Inst., Univ. Heidelberg, Germany. ICDD Grant-in-Aid, 1995.
56 Y. H. Jin, Y. H. Hu, L. Chen, X. J. Wang, Z. F. Mu, G. F. Ju and Z. F. Yang, *Phys. B*, 2014, **436**, 105–110.
57 H. B. Liang, Y. Tao and Q. Su, *Mater. Sci. Eng., B*, 2005, **119**, 152–158.
58 J. Y. Sun, Y. N. Sun, J. H. Zeng and H. Y. Du, *J. Phys. Chem. Solids*, 2013, **74**, 1007–1011.

59 J. Y. Sun, Y. N. Sun, J. H. Zeng and H. Y. Du, *Opt. Mater.*, 2013, **35**, 1276–1278.
60 N. Guo, Y. H. Zheng, Y. C. Jia, H. Qiao and H. P. You, *New J. Chem.*, 2012, **36**, 168–172.
61 J. Y. Sun, J. H. Zeng, Y. N. Sun and H. Y. Du, *J. Alloys Compd.*, 2012, **540**, 81–84.
62 C. M. Smith, Penn State University, University Park, Pennsylvania, USA, ICDD Grant-in-Aid, 1976.
63 V. B. Mikhailik and H. Kraus, *J. Lumin.*, 2009, **129**, 945–947.
64 P. L. Shi, Z. G. Xia, M. S. Molokeev and V. V. Atuchin, *Dalton Trans.*, 2014, **43**, 9669–9676.
65 F. Baur, F. Glocker and T. Jüstel, *J. Mater. Chem. C*, 2015, **3**, 2054.